A&A 642, A230 (2020)
https://doi.org/10.1051/0004-6361/202038714

Astronomy & Astrophysics

Period–luminosity–metallicity relation of classical Cepheids*

V. Ripepi[1], G. Catanzaro[2], R. Molinaro[1], M. Marconi[1], G. Clementini[3], F. Cusano[3], G. De Somma[1,4,5], S. Leccia[1], I. Musella[1], and V. Testa[6]

[1] INAF-Osservatorio Astronomico di Capodimonte, Salita Moiariello 16, 80131 Naples, Italy
e-mail: vincenzo.ripepi@inaf.it
[2] INAF-Osservatorio Astrofisico di Catania, Via S.Sofia 78, 95123 Catania, Italy
[3] INAF-Osservatorio di Astrofisica e Scienza dello Spazio, Via Gobetti 93/3, 40129 Bologna, Italy
[4] Dipartimento di Fisica "E. Pancini", Università di Napoli "Federico II", Via Cinthia, 80126 Napoli, Italy
[5] Istituto Nazionale di Fisica Nucleare (INFN)-Sez. di Napoli, Via Cinthia, 80126 Napoli, Italy
[6] INAF – Osservatorio Astronomico di Roma, Via Frascati 33, 00078 Monte Porzio Catone, Italy

Received 22 June 2020 / Accepted 6 August 2020

ABSTRACT

Context. Classical Cepheids (DCEPs) are the most important primary indicators for the extragalactic distance scale. Establishing the dependence on metallicity of their period–luminosity and period–Wesenheit (PL and PW) relations has deep consequences for the estimate of the Hubble constant (H_0).
Aims. We investigate the dependence on metal abundance ([Fe/H]) of the PL and PW relations for Galactic DCEPs.
Methods. We combined proprietary and literature photometric and spectroscopic data, gathering a total sample of 413 Galactic DCEPs (372 fundamental mode, DCEP_F, and 41 first-overtone, DCEP_1O) and constructed new metallicity-dependent PL and PW relations in the near-infrared adopting the astrometry-based luminosity.
Results. We find indications that the slopes of the PL(K_S) and PW(J, K_S) relations for Galactic DCEPs might depend on metallicity on the basis of the comparison with the Large Magellanic Cloud relationships. Therefore we used a generalized form of the PL and PW relations to simultaneously take the metallicity dependence of the slope and intercept of these relations into account.
Conclusions. We calculated PL and PW relations that for the first time explicitly include a metallicity dependence of the slope and intercept terms. The quality of the available data is insufficient, however, and we cannot yet present conclusive results, but they are relevant from a methodological point of view. The new relations are linked to the geometric measurement of the distance to the Large Magellanic Cloud and allowed us to estimate a *Gaia* DR2 parallax zero-point offset $\Delta\varpi = 0.0615 \pm 0.004$ mas from the dataset of DCEPs used in this work.

Key words. stars: variables: Cepheids – stars: distances – distance scale – stars: abundances – stars: fundamental parameters

1. Introduction

Classical Cepheids (DCEPs) are the most important primary distance indicators of the cosmic distance ladder through their period-luminosity (PL, Leavitt & Pickering 1912) and period-Wesenheit (PW, Madore 1982) relations. When they are calibrated locally by means of geometric methods such as trigonometric parallaxes, the PL and PW relations can be used to calibrate secondary distance indicators such as type Ia supernovae (SNe), which are sufficiently powerful to measure distances in the unperturbed Hubble flow. This three-step procedure eventually allows us to measure the Hubble constant (H_0) from the slope of the relation between the distance to far-away galaxies in the Hubble flow and their recession velocity (e.g. Sandage et al. 2006; Freedman & Madore 2011; Freedman et al. 2012; Riess et al. 2016, 2019).

The value of H_0 currently is a matter of vivid debate in the literature because the most recent determinations based on the cosmic distance ladder, $H_0 = 74.03 \pm 1.42$ km s^{-1} Mpc^{-1} (Riess et al. 2019 and references therein), significantly disagree with the value of H_0 estimated from the *Planck* cosmic microwave background (CMB) measurements under the flat Λ cold dark matter (ΛCDM) model, $H_0 = 67.4 \pm 0.5$ km s^{-1} Mpc^{-1} (Planck Collaboration VI 2020). This 4.4σ discrepancy, commonly referred to as the H_0 tension, remains unexplained despite several attempts to reduce the systematic errors affecting the different steps of the cosmic distance ladder (e.g. Huang et al. 2020; Yuan et al. 2019; Reid et al. 2019). Recently, a value of $H_0 = 73.3^{+1.7}_{-1.8}$ km s^{-1} Mpc^{-1}, in agreement with the cosmic distance ladder, was obtained by the H0LICOW and STRIDES collaborations based on the gravitational time-delays of six lensed quasars (Wong et al. 2020). Because this measurement is entirely independent of cosmic distance ladder calibrations, the occurrence of a tension appears to be confirmed. In order to improve the accuracy of the H_0 measurements and to place stringent constraints on cosmological models, it is crucial to quantify the residual systematic errors affecting different methods to estimate H_0. In particular, it is mandatory to quantify and reduce the uncertainties (random and systematic) of the different steps involved in the distance ladder calibration.

One of the main residual sources of uncertainty in the cosmic distance ladder is the metallicity dependence of the DCEP PL and PW relations. The metallicity is widely expected to affect the slope and intercept of the DCEP PL and PW relations,

* Based on observations made with the Italian Telescopio Nazionale *Galileo* (TNG) operated by the Fundación Galileo Galilei (FGG) of the Istituto Nazionale di Astrofisica (INAF) at the Observatorio del Roque de los Muchachos (La Palma, Canary Islands, Spain).

particularly at optical passbands. Conversely, the metallicity dependence of the DCEP PW relations is estimated and predicted to be weak for different band combinations, but especially in the near-infrared (NIR, see e.g. Fiorentino et al. 2007, 2013; Ngeow et al. 2012; Di Criscienzo et al. 2013; Gieren et al. 2018, and references therein).

The procedure adopted by the SH0ES team (Riess et al. 2016) to calibrate the cosmic distance ladder takes the metallicity dependence of the PW relations into account. According to these authors, the metallicity contributes 0.5% to the total error budget of 2.4% in the measure of H_0. However, the estimates for the metallicity dependence of the PL and PW relations obtained by different authors disagree significantly (e.g. Macri et al. 2006; Romaniello et al. 2008; Bono et al. 2010; Freedman & Madore 2011; Shappee & Stanek 2011; Pejcha & Kochanek 2012; Groenewegen 2013; Kodric et al. 2013; Fausnaugh et al. 2015; Riess et al. 2016). This variety of results can be partially explained by the significant errors that still affect the metal abundances of DCEPs in the distant galaxies that are addressed in these studies.

A direct determination of the metallicity effect on the Cepheid distance scale, based on Galactic DCEPs with [Fe/H] abundances obtained from high-resolution spectroscopy, has been hampered until recently by the lack of precise distance measurements for a sufficiently large number of Mikly Way (MW) DCEPs. In this context, a unique contribution is today provided by the *Gaia* mission (Gaia Collaboration 2016), which published in its Data Release 2 (DR2) precise parallaxes for hundreds of MW DCEPs, including most of the new discoveries in the last several years (see e.g. Chen et al. 2018; Jayasinghe et al. 2018; Udalski et al. 2018; Clementini et al. 2019; Ripepi et al. 2019). Further improved parallaxes are foreseen to be provided by future *Gaia* data releases.

However, only a small fraction of the recently discovered DCEPs have accurate multiband photometry and spectroscopic abundances. To fully exploit the potential of such an ideal amount of data and to better estimate the metallicity dependence of the DCEP PL and PW relations, it is therefore crucial to increase the sample of well-characterized (in photometry and spectroscopy) MW DCEPs. To this end, we are carrying out a project that combines the multiband photometry availble in the literature with metal abundances from newly acquired high-resolution spectroscopy for more than one hundred MW DCEPs, selected among the new discoveries and those that are poorly characterised in the literature so far. First results from this project were published in Catanzaro et al. (2020), where we presented a new lithium-rich DCEP, V363 Cas, the fifth of this rare class of DCEPs to be discovered in the MW, and in Ripepi et al. (in prep., hereinafter Paper I) where we presented elemental abundances from high-resolution spectroscopy for a first sample of 21 DCEPs and a type II Cepheid of BL Herculis (BL Her) type among the more than 100 DCEPs we target with our observing program. In this paper we exploit the iron abundances published in Paper I along with literature data to study the metallicity dependence of the NIR PL and PW relations for MW DCEPs.

2. Sample

In Paper I we presented chemical abundances and photometric properties for a sample of 21 DCEPs and one BL Her star[1]. This sample was complemented with homogeneous literature data from Gaia Collaboration (2017) and Groenewegen (2018). A detailed description of the properties of our total sample can be found in Paper I. Here we only recall that it consists of 389 fundamental-mode (DCEP_F) and 44 first-overtone (DCEP_1O) classical Cepheids. Of these, those with RUWE ≥ 1.4 were discarded as recommended by the *Gaia* documentation[2]. Similarly, we removed the DCEPs with $V < 6$ mag, as their *Gaia* parallaxes are too uncertain (see Riess et al. 2018). The literature sample was hence reduced to 364 DCEP_F and 38 DCEP_1O pulsators. Adding the 9 DCEP_F and 12 DCEP_1O pulsators studied in Paper I, our final sample consisting of 373 DCEP_Fs and 50 DCEP_1Os.

3. Period-luminosity-metallicity and period-Wesenheit-metallicity relations in the NIR for the Galactic DCEPs

We used our final sample of 373 DCEP_Fs and 50 DCEP_1Os to derive a new PL relation in the K_S band and a new PW relation in the J, K_S bands. First, we obtained dereddened $K_{S,0}$ magnitudes that are required to construct the PL_{K_S} relation by adopting $A_{K_S} = 0.34\,E(B-V)$ (as derived by Cardelli et al. 1989, using $R_V = 3.1$), where the $E(B-V)$ values are those collected in Paper I. The corresponding Wesenheit magnitudes $w = Ks - 0.69\,(J-K_S)$ are instead reddening-free by construction.

To avoid introducing any bias or sample truncation, we did not make any selection of the DCEPs based on their parallax and/or the ratio of parallax error over parallax, which means that we also retained a few objects with negative parallax. To handle the negative parallaxes as well, we adopted the approach introduced by Feast & Catchpole (1997) and Arenou & Luri (1999), and computed the astrometry-based luminosity (ABL), which in the simplest case is defined as follows:

$$\mathrm{ABL} = 10^{0.2M_{K_{S,0}}} = 10^{0.2[\alpha+\beta(\log P - \log P_0)]} = \varpi 10^{0.2K_{S,0}-2} \quad (1)$$

$$\mathrm{ABL} = 10^{0.2W} = 10^{0.2[\alpha+\beta(\log P - \log P_0)]} = \varpi 10^{0.2w(J,K_S)-2}, \quad (2)$$

where $K_{S,0}$, $w(J, K_S)$, the period P, and the parallax ϖ are the observables; the unknowns are the two parameters α and β that define the absolute quantity $M_{\rm abs} = \alpha + \beta(\log P - \log P_0)$, which corresponds to the absolute magnitude $M_{K_{S,0}}$ in Eq. (1) and to the absolute Wesenheit magnitude $W(J, K_S)$ in Eq. (2). We used a pivoting (logarithmic) period P_0 of 1.0 ($P_0 = 10$ d) for DCEP_Fs and 0.3 ($P_0 = 2$ d) for DCEP_1Os to reduce the correlation between the parameters of the fit. The α and β values were calculated by a weighted least-squares fit procedure with σ-clipping of the residuals, adopting a double median absolute deviation (MAD) with amplitude = 4.5 MAD to limit the maximum number of rejected objects to ~10%. Uncertainties were estimated through a bootstrap technique. The fit of the ABL function was carried out by adopting three different values for the offset of the *Gaia* parallax zero-point, $\Delta\varpi = 0.049$ mas, following Groenewegen (2018), $\Delta\varpi = 0.07$ mas according to Ripepi et al. (2019), and a third intermediate value: $\Delta\varpi = 0.0615$ mas (see Sect. 5). We refer to Groenewegen (2018) and Ripepi et al. (2019) for a discussion of the *Gaia* parallax zero-point offset for DCEPs (see also Arenou et al. 2018; Lindegren et al. 2018, for a more general discussion of the topic). The results of the fitting procedure are shown in Fig. 1, where we have highlighted the DCEPs analysed in Paper I with different symbols.

[1] Star ASAS J162326-0941.0, was previously classified as DCEP.

[2] The RUWE parameter measures the reliability of the *Gaia* parallaxes, see Sect. 14.1.2 of "*Gaia*" Data Release 2 Documentation release 1.2"; https://gea.esac.esa.int/archive/documentation/GDR2/

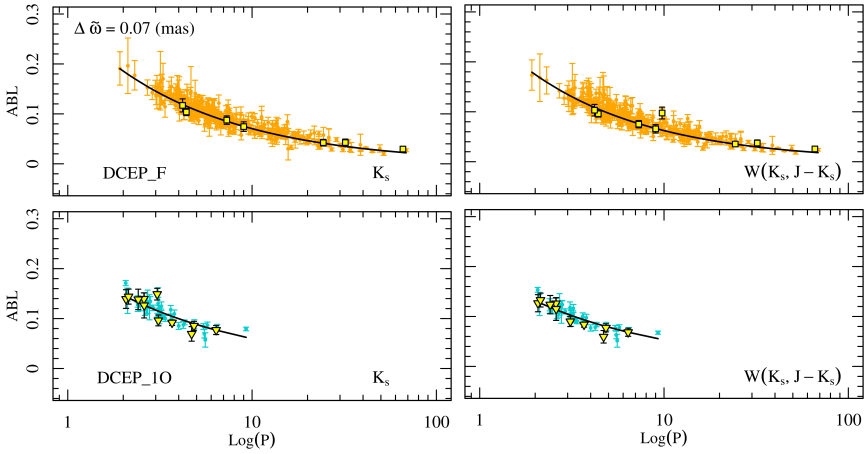

Fig. 1. Results of the fitting procedure for an ABL in the form of Eq. (1) (*left*) and Eq. (2) (*right*) for DCEP_Fs (*top panels*) and DCEP_1Os (*bottom panels*) and a *Gaia* zero-point parallax offset of $\Delta\varpi = 0.07$ mas. The filled orange and cyan circles represent the literature data for F and 1O MW DCEPs, respectively. Filled yellow squares and triangles display the DCEP_Fs and DCEP_1Os analysed in Paper I, respectively. For clarity reasons, outliers were not shown.

Table 1. Results from the least-squares fit of an ABL function in the form of Eqs. (1) and (2) (upper portion of the table); Eqs. (3) and (4) (middle portion of the table), or Eqs. (5) and (6) (lower part of the table).

α (1)	β (2)	γ (3)	δ (4)	n (5)	$n_{\rm rej}$ (6)	Mode (7)	$\Delta\varpi$ (8)	Case (9)	$\sigma_{\rm ABL}$ (10)	AIC (11)
$M_{K_{S,0}}$ or $W(J,K_S) = \alpha + \beta(\log P - \log P_0)$										
-5.840 ± 0.023	-3.061 ± 0.070	–	–	373	47	F	0.0490	(K)	0.0095	−2594
-5.794 ± 0.021	-3.027 ± 0.090	–	–	373	55	F	0.0615	(K)	0.0091	−2533
-5.762 ± 0.028	-3.012 ± 0.086	–	–	373	53	F	0.0700	(K)	0.0098	−2533
-6.131 ± 0.027	-3.219 ± 0.078	–	–	373	45	F	0.0490	(K, JK)	0.0091	−2666
-6.072 ± 0.024	-3.185 ± 0.085	–	–	373	51	F	0.0615	(K, JK)	0.0086	−2635
-6.027 ± 0.016	-3.200 ± 0.087	–	–	373	40	F	0.0700	(K, JK)	0.0090	−2631
-4.223 ± 0.082	-2.836 ± 0.474	–	–	50	2	1O	0.0490	(K)	0.0109	−366
-4.190 ± 0.117	-2.788 ± 0.533	–	–	50	2	1O	0.0615	(K)	0.0101	−364
-4.166 ± 0.091	-2.780 ± 0.453	–	–	50	2	1O	0.0700	(K)	0.0107	−365
-4.457 ± 0.101	-2.889 ± 0.425	–	–	50	2	1O	0.0490	(K, JK)	0.0091	−382
-4.430 ± 0.092	-2.786 ± 0.371	–	–	50	5	1O	0.0615	(K, JK)	0.0078	−363
-4.404 ± 0.082	-2.802 ± 0.428	–	–	50	4	1O	0.0700	(K, JK)	0.0087	−370
$M_{K_{S,0}}$ or $W(J,K_S) = \alpha + \beta(\log P - \log P_0) + \gamma$[Fe/H]										
-5.837 ± 0.030	-3.053 ± 0.093	-0.039 ± 0.151	–	373	46	F	0.0490	(K)	0.0096	−2600
-5.785 ± 0.027	-3.015 ± 0.089	-0.082 ± 0.138	–	373	55	F	0.0615	(K)	0.0091	−2532
-5.746 ± 0.022	-2.992 ± 0.077	-0.141 ± 0.140	–	373	54	F	0.0700	(K)	0.0098	−2527
-6.121 ± 0.027	-3.216 ± 0.067	-0.084 ± 0.145	–	373	41	F	0.0490	(K, JK)	0.0093	−2684
-6.033 ± 0.029	-3.171 ± 0.065	-0.284 ± 0.115	–	373	34	F	0.0615	(K, JK)	0.0093	−2698
-5.991 ± 0.027	-3.148 ± 0.069	-0.356 ± 0.171	–	373	33	F	0.0700	(K, JK)	0.0098	−2686
-4.237 ± 0.128	-2.869 ± 0.641	0.225 ± 0.255	–	50	1	1O	0.0490	(K)	0.0108	−368
-4.204 ± 0.106	-2.787 ± 0.426	0.161 ± 0.295	–	50	3	1O	0.0615	(K)	0.0098	−357
-4.175 ± 0.107	-2.739 ± 0.517	0.101 ± 0.298	–	50	5	1O	0.0700	(K)	0.0088	−341
-4.447 ± 0.120	-2.893 ± 0.412	-0.111 ± 0.228	–	50	2	1O	0.0490	(K, JK)	0.0101	−381
-4.408 ± 0.108	-2.788 ± 0.427	-0.253 ± 0.230	–	50	5	1O	0.0615	(K, JK)	0.0082	−363
-4.381 ± 0.099	-2.761 ± 0.484	-0.304 ± 0.254	–	50	5	1O	0.0700	(K, JK)	0.0079	−362
$M_{K_{S,0}}$ or $W(J,K_S) = \alpha + (\beta + \delta$[Fe/H]$)(\log P - \log P_0) + \gamma$[Fe/H]										
-5.837 ± 0.023	-3.064 ± 0.101	-0.044 ± 0.170	0.086 ± 0.673	373	49	F	0.0490	(K)	0.0096	−2579
-5.771 ± 0.030	-3.112 ± 0.111	-0.185 ± 0.191	0.704 ± 0.650	373	30	F	0.0615	(K)	0.0111	−2626
-5.731 ± 0.033	-3.111 ± 0.095	-0.256 ± 0.158	0.866 ± 0.587	373	27	F	0.0700	(K)	0.0113	−2607
-6.130 ± 0.035	-3.274 ± 0.117	-0.078 ± 0.164	0.507 ± 0.528	373	38	F	0.0490	(K, JK)	0.0096	−2690
-6.044 ± 0.025	-3.234 ± 0.118	-0.237 ± 0.157	0.465 ± 0.592	373	35	F	0.0615	(K, JK)	0.0096	−2698
-6.005 ± 0.025	-3.241 ± 0.093	-0.283 ± 0.160	0.727 ± 0.564	373	26	F	0.0700	(K, JK)	0.0103	−2716

Notes. The functional form of the PW relation is labelled in the table. P_0 is the pivoting period, whose logarithm is equal to 1.0 and 0.3 for DCEP_Fs and DCEP_1Os, respectively. The different columns provide (1–4) coefficients of the non-linear fit and their relative errors; (5–6) total number of available DCEPs and number of sources rejected during the fitting procedure; (7) pulsation mode; (8) adopted *Gaia* parallax offset (in mas); (9) case; (10) rms of the residuals of the ABL function; (11) AIC value (see text).

The coefficients of the fit of Eqs. (1) and (2) are provided in the upper portion of Table 1. We first compare our results with the PL and PW relations defined by the Large Magellanic Cloud (LMC) DCEPs, which are based on large samples and therefore have very precise slopes (and intercepts). We used as a reference the PL(K_S) relations by Ripepi et al. (2012) and the PW(J, K_S)

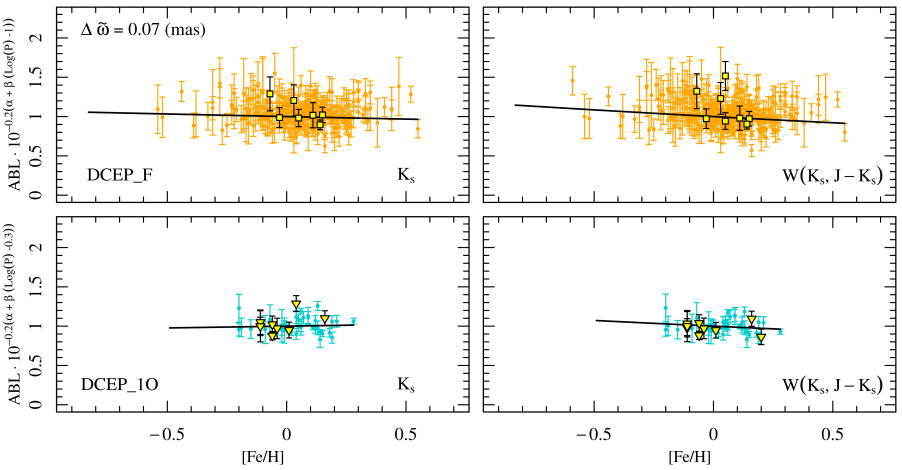

Fig. 2. Results of the fitting procedure for an ABL in the form of Eq. (3) (*left*) and Eq. (4) (*right*) for DCEP_Fs (*top panels*) and DCEP_1Os (*bottom panels*) and a *Gaia* zero-point parallax offset of $\Delta\varpi = 0.07$ mas. Symbols are the same as in Fig. 1.

relations by Ripepi et al. (2020), which are based on the NIR time-series photometry collected by the Vista Magellanic Cloud Survey (VMC Cioni et al. 2011)[3]. In particular, in the LMC these authors find PL and PW slopes of $\Delta K_S/\Delta \log P = -3.295 \pm 0.018$ and $\Delta w(J, K_S)/\Delta \log P = -3.332 \pm 0.007$ for the DCEP_Fs, and $\Delta K_S/\Delta \log P = -3.471 \pm 0.035$ and $\Delta w(J, K_S)/\Delta \log P = -3.501 \pm 0.007$ for the DCEP_1Os. A comparison with the values in the upper part of Table 1 allows us to make the following considerations:

– Despite an increase by 12 units of the Galactic DCEP_1O sample provided by Paper I, their number is still too small to allow for precise results. For any value of the parallax zero-point offset, the slopes (β) of our MW PL and PW relations are significantly lower than for the LMC DCEP_1Os and errors are very large.

– The PL and PW relations of the MW DCEP_Fs both show meaningful slopes with reasonably small errors. For all the values of $\Delta\varpi$, these slopes appear to be significantly lower than for the LMC DCEPs. The discrepancy is at the 3σ level for the PL relation. Because the average metallicity of the MW and LMC DCEPs differs by some ∼0.3−0.4 dex, we can expect that metallicity may play a role in explaining these differences.

To test this possibility, we added a metallicity term to the intercept of the PL and PW relations. In this case, the ABL formulation becomes

$$\mathrm{ABL} = 10^{0.2M_{K_{S,0}}} = 10^{0.2\{\alpha+\beta(\log P-\log P_0)+\gamma[\mathrm{Fe/H}]\}} = \varpi 10^{0.2K_{S,0}-2} \quad (3)$$

$$\mathrm{ABL} = 10^{0.2W} = 10^{0.2\{\alpha+\beta(\log P-\log P_0)+\gamma[\mathrm{Fe/H}]\}} = \varpi 10^{0.2w(J,K_S)-2}. \quad (4)$$

We adopted the same procedure as above to fit Eqs. (3) and (4) to the data, obtaining the coefficients listed in the middle portion of Table 1. Analysing these results, we note that (i) for the DCEP_Fs the metallicity term is negative and generally increasingly significant as $\Delta\varpi$ increases, especially for the PW relation; for the DCEP_1Os the results seem to show the same general trend (but the dependence is positive for the PL relation). However, the errors on the slopes and intercepts of the DCEP_1O relations are up to one order of magnitude larger than for the DCEP_Fs; (ii) for the DCEP_Fs, the slopes of both the PL and PW relations do not change significantly, decrease slightly and thus become increasingly different than those of the LMC. The decrement is larger as the metallicity term increases, revealing an intricate inter-dependency between these parameters. In any case, we conclude that the slopes of the PL and PW relations for the MW DCEPs differ from those of the LMC DCEPs and seem to exhibit a non-negligible metallicity dependence.

More in general, our results seem to indicate that there is a complicate interplay between the metallicity dependence caused by the higher average metallicity of the MW DCEPs with respect to the LMC DCEPs, the coefficients of the PL and PW relations, and the zero-point offset of the *Gaia* parallaxes. In order to possibly shed light on this rather intricate scenario, we adopted a more general form of the PL and PW relations that takes a metallicity dependence not only of the intercept, but also of the period coefficient into account. This was rendered through the following general ABL functions:

$$\mathrm{ABL} = 10^{0.2(\alpha+(\beta+\delta[\mathrm{Fe/H}])(\log P-\log P_0)+\gamma[\mathrm{Fe/H}])} = \varpi 10^{0.2K_{S,0}-2} \quad (5)$$

$$\mathrm{ABL} = 10^{0.2(\alpha+(\beta+\delta[\mathrm{Fe/H}])(\log P-\log P_0)+\gamma[\mathrm{Fe/H}])} = \varpi 10^{0.2w(J,K_S)-2}, \quad (6)$$

which we proceeded to fit in exactly the same way as done in the previous cases, but considering only the DCEP_F pulsators because there are too few DCEP_1Os for us to obtain meaningful results. The outcomes of this procedure are summarised in the bottom portion of Table 1 and shown in Fig. 3 (top and medium panels). We note a general behaviour similar to the previous case: the metallicity dependence on intercept and slope increases as $\Delta\varpi$ increases. In no case are the metallicity terms significant for $\Delta\varpi = 0.049$ mas, whereas the maximum significance is achieved for $\Delta\varpi = 0.070$ mas, when the PL and PW relations show metallicity terms that are significant at 1-2σ levels. In the intermediate case, $\Delta\varpi = 0.0615$ mas, the metallicity dependence is significant at $\sim 1\sigma$ level. To summarise, even if the uncertainties are still rather large, and except for the PL and PW relations with $\Delta\varpi = 0.049$ mas, it was possible to find a meaningful metallicity dependence for the slope (period coefficient) and intercept. This is the first time to our knowledge that such a result is achieved, even though it still is more qualitative than quantitative evidence. We also note that the metallicity dependence of the slope appears to have the right sign, suggesting smaller slopes as [Fe/H] increases, as inferred from the comparison of LMC and MW DCEPs and in remarkable agreement with the predictions of non-linear convective pulsation models (see e.g. Bono et al. 1999; Marconi et al. 2005, and references therein).

4. Goodness of fit

In Sect. 3 we performed several fits of the ABL function with an increasing number of coefficients to take the metallicity

[3] Similar results were obtained by other authors (e.g. Inno et al. 2016).

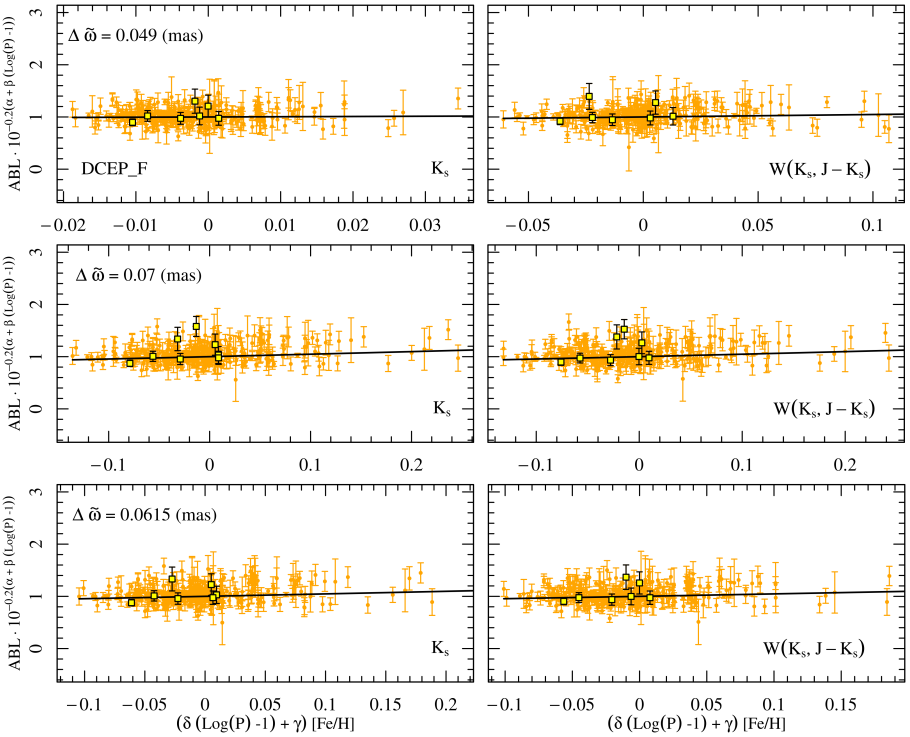

Fig. 3. Same as in Fig. 2, but fitting an ABL in the general form of Eq. (5) (*left panels*) and Eq. (6) (*right panels*) for three different choices of the *Gaia* parallax zero-point offset. The fit is presented only for fundamental-mode pulsators as no sensible fit could be performed of the DCEP_1Os because our sample contains so few of them.

dependence into account, and for different values of $\Delta\varpi$, obtaining comparable values of the ABL function residuals. Prompted by the referee, we now try to obtain an indication of the goodness of these fits. We chose to adopt the commonly used Akaike information criterion (AIC, Akaike 2011)[4]. We first calculated the likelihood of each of the fitted ABL functions. Therefore we define

$$\ln \mathcal{L} = -0.5 \sum_{i=1}^{N} \left[\left(\frac{\mathrm{res}_i}{s_i} \right)^2 + \ln(s_i^2) \right], \quad (7)$$

where N is the number of fitted points, res_i is the ith residual around the fitted relations (Eqs. (1)–(6) above), and the term s_i is the sum in quadrature of the ith uncertainty and the intrinsic scatter around the fitted relation. We set the intrinsic scatter of the fitted relations equal to half the rms of the residuals, but verified that this choice did not affect the results significantly. The values of the likelihood were then used to estimate the AIC quantity, which is defined as

$$\mathrm{AIC} = 2k - 2 \ln \mathcal{L}, \quad (8)$$

where k is the number of fitted parameters. The AIC values are reported in the last column of Table 1. By definition, the lower the AIC value, the better the fit. An analysis of Table 1 reveals that introducing the metallicity terms on the intercept and slope has different effects on the PL and PW relations. Specifically, the introduction of a metallicity term on the intercept of the PL relation does not improve the fit to the data significantly, whereas the inclusion of a metallicity dependence for both coefficients seems to improve the fit since, except for $\Delta\varpi = 0.049$ mas, the coefficients of the PL relation become more than $\sim 1\sigma$ significant. The introduction of the metallicity term on the intercept improves the PW relation fit. The adoption of the metallicity term on the slope as well produces a slightly better or equal goodness of fit. The best value of the AIC is obtained for the PW relation with $\Delta\varpi = 0.070$ mas.

In summary, use of the AIC goodness-of-fit parameter allowed us to verify that the progressive inclusion of the metallicity term in the intercept and slope of the PL and PW relations produces fits to the data that except in the case of $\Delta\varpi = 0.049$ mas, are generally (slightly) better than the cases when fewer parameters are used to define the ABL function.

5. Discussion and concluding remarks

We tested our PL and PW relations by applying them to the LMC DCEP_F sample in Ripepi et al. (2020) and comparing the resulting LMC distance modulus ($\mathrm{DM_{LMC}}$) to the distance to the LMC provided by the geometric determination of Pietrzyński et al. (2019): $\mathrm{DM_{LMC}} = 18.48 \pm 0.03$ mag (including systematic errors), which is currently considered one of the most accurate measures in the literature. We calculated the absolute $M_{K_{0,S}}$ and Wesenheit magnitudes $W(J, K_S)$ for each LMC DCEP_F in Ripepi et al. (2020) by inserting the proper periods in the respective equations in Table 1 for the three different cases: (i) with only the coefficients α and β, (ii) with the addition of the γ term, and (iii) with the further addition of the δ coefficient. In cases (i) and (ii) we implicitly assumed that there is no difference in the slope (period term) of the PL and PW relations of the MW and LMC DCEPs. In cases (ii) and (iii) we adopted an average metallicity for the LMC DCEPs of $\langle$[Fe/H]$\rangle = -0.33$ dex from Romaniello et al. (2008). In all three cases, from the observed $K_{0,S}$ and $w(J, K_S)$ we obtained individual DM values for each LMC DCEP_F. The distributions of these DMs are shown in Fig. 4 from top to bottom for the three cases (i)−(iii) and from left to the right for the three adopted values of $\Delta\varpi = 0.049$, 0.0615, and 0.070 mas, respectively. In each panel we compare the DM distributions with the LMC geometric distance by Pietrzyński et al. (2019). In all cases the histograms

[4] We also calculated the Bayesian information criterion (BIC), which produced results very similar to the AIC, therefore we only report and discuss the latter here.

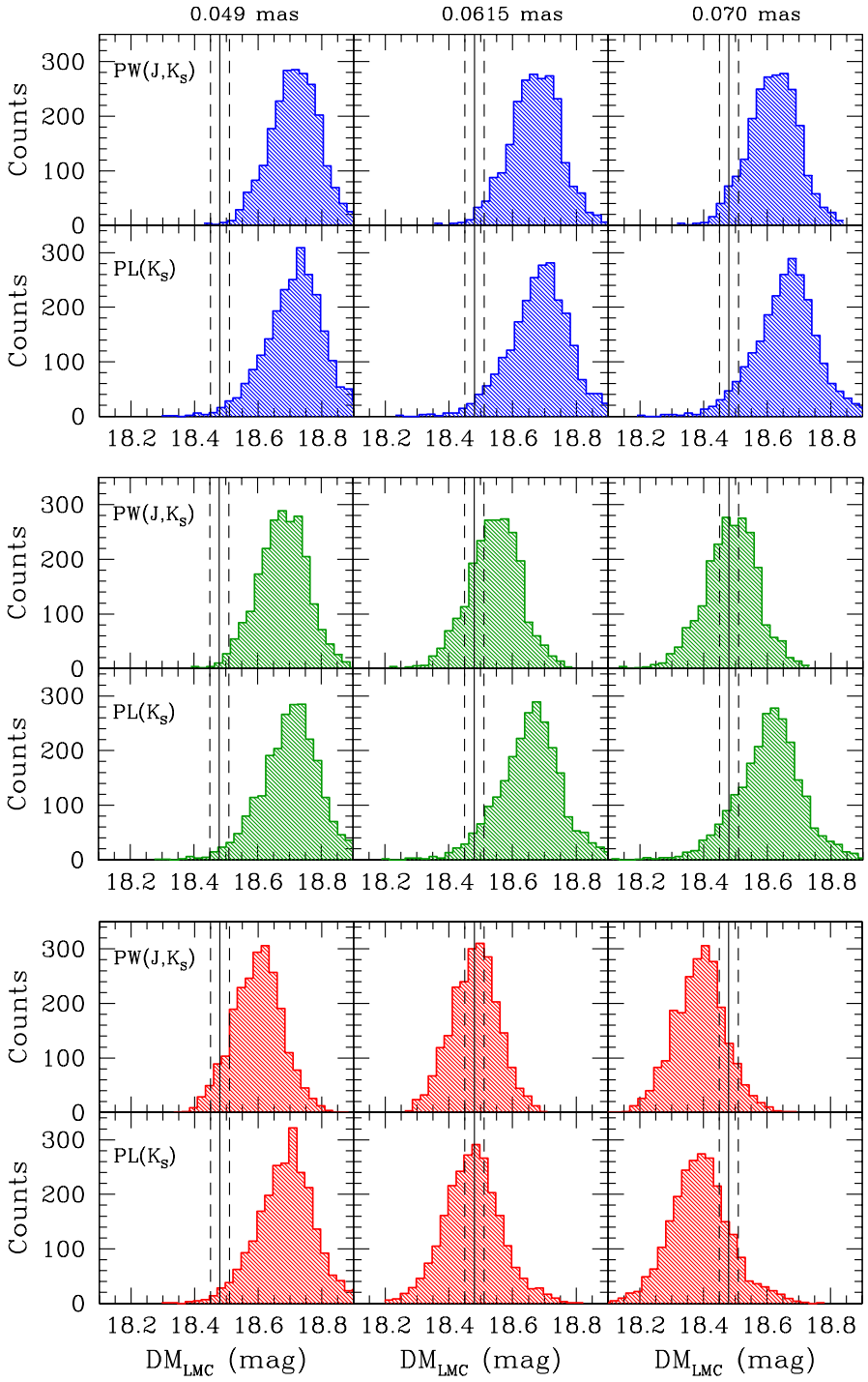

Fig. 4. Distribution of the individual DMs for DCEP_Fs in the LMC based on distances calculated using (i) the ABL in the form of Eqs. (1) and (2) (*top panels*, blue histograms), (ii) the ABL in the form of Eqs. (3) and (4) (middle panels, green histograms), (iii) the ABL in the form of Eqs. (5) and (6) (*bottom panels*, red histograms), and the NIR photometry of the VMC survey (see text for details). *From left to right*: the different panels show results obtained for three different values of the *Gaia* parallax zero-point offset: $\Delta\varpi = 0.049$, 0.0615 and 0.070 mas. The vertical solid line shows the LMC distance modulus by Pietrzyński et al. (2019); the dashed lines represent its 1σ uncertainty.

show rather narrow distributions; the average dispersion is about 0.08−0.09 mag.

The top panels of Fig. 4 (blue histograms) show that in all cases, solution (i), no metallicity dependence, provides $\langle DM_{LMC}\rangle$ values that are far higher than the LMC geometric distance by Pietrzyński et al. (2019). A significantly larger $\Delta\varpi$ offset would be needed to reconcile the two results. The middle panels of Fig. 4 (green histograms) corresponding to case (ii) (metallicity dependence only on the intercept) still provide too high $\langle DM_{LMC}\rangle$ values, except in the case of the PW relation with $\Delta\varpi = 0.070$ mas, which has the largest difference in slope with respect to the observed LMC PW relation, however. Finally, the bottom panels of Fig. 4 (red histograms), corresponding to case (iii) (metallicity dependence of both slope and intercept), agree very well with the $\langle DM_{LMC}\rangle$ value by Pietrzyński et al. (2019) for $\Delta\varpi = 0.0615$ mas, whereas the other two values of $\Delta\varpi$ produce either lower or higher $\langle DM_{LMC}\rangle$ estimates.

This shows that the general formulation of the PL and PW relations is not only able to qualitatively explain the different slopes of the PL and PW relations in the MW and LMC, but also allows us to obtain an estimate of the zero-point offset of the *Gaia* DR2 parallaxes for DCEPs. An error on the offset value can be inferred from the uncertainty on the LMC distance modulus by Pietrzyński et al. (2019). This corresponds to 0.03 mag, which translates into a 0.004 mas error in the parallax offset. Our best estimate for the *Gaia* DR2 zero-point parallax offset for

our DCEP dataset therefore is 0.0615 ± 0.004 mas. It is important to remark that this zero-point offset has to be considered as an average that is valid only for the particular DCEP dataset used here because in general, the zero-point offset of the *Gaia* parallaxes varies for different groups of objects and different positions in the sky (see e.g. Arenou et al. 2018; Lindegren et al. 2018; Leung & Bovy 2019).

To conclude, the general PL and PW relations provided in the bottom part of Table 1 could represent a step forward in our ability to measure distances through DCEPs, with a potential great effect on the cosmic distance scale and the estimate of H_0. Additional spectroscopic measurements for DCEPs in the MW and the LMC, as well as more precise parallaxes expected from the forecoming *Gaia* Early Data Release 3, will be fundamental to confirm the results presented in this paper.

Acknowledgements. We wish to thank the anonymous referee for his/her suggestions, which helped to improve the paper. This work has made use of data from the European Space Agency (ESA) mission *Gaia* (https://www.cosmos.esa.int/gaia), processed by the *Gaia* Data Processing and Analysis Consortium (DPAC, https://www.cosmos.esa.int/web/gaia/dpac/consortium). Funding for the DPAC has been provided by national institutions, in particular the institutions participating in the *Gaia* Multilateral Agreement. In particular, the Italian participation in DPAC has been supported by Istituto Nazionale di Astrofisica (INAF) and the Agenzia Spaziale Italiana (ASI) through grants I/037/08/0, I/058/10/0, 2014-025-R.0, and 2014-025-R.1.2015 to INAF (PI M.G. Lattanzi). V.R., M.M. and G.C. acknowledge partial support from the project "MITiC: MIning The Cosmos Big Data and Innovative Italian Technology for Frontier Astrophysics and Cosmology" (PI B. Garilli). RM thanks his wife and her parents that made possible his collaboration to this work during the current pandemic period.

References

Akaike, H. 2011, in Akaike's Information Criterion, ed. M. Lovric (Berlin, Heidelberg: Springer), Int. Encycl. Stat. Sci.
Arenou, F., & Luri, X. 1999, Harmonizing Cosmic Distance Scales in a Post-HIPPARCOS Era, 167, 13
Arenou, F., Luri, X., Babusiaux, C., et al. 2018, A&A, 616, A17
Bono, G., Caputo, F., Castellani, V., et al. 1999, ApJ, 512, 711
Bono, G., Caputo, F., Marconi, M., et al. 2010, ApJ, 715, 277
Cardelli, J. A., Clayton, G. C., & Mathis, J. S. 1989, ApJ, 345, 245
Catanzaro, G., Ripepi, V., Clementini, G., et al. 2020, A&A, 639, L4
Chen, X., Wang, S., Deng, L., et al. 2018, ApJS, 237, 28
Cioni, M.-R. L., Clementini, G., Girardi, L., et al. 2011, A&A, 527, A116
Clementini, G., Ripepi, V., Molinaro, R., et al. 2019, A&A, 622, A60
Di Criscienzo, M., Marconi, M., Musella, I., Cignoni, M., & Ripepi, V. 2013, MNRAS, 428, 212
Fausnaugh, M. M., Kochanek, C. S., Gerke, J. R., et al. 2015, MNRAS, 450, 3597
Feast, M. W., & Catchpole, R. M. 1997, MNRAS, 286, L1
Fiorentino, G., Marconi, M., Musella, I., & Caputo, F. 2007, A&A, 476, 863
Fiorentino, G., Musella, I., & Marconi, M. 2013, MNRAS, 434, 2866
Freedman, W. L., & Madore, B. F. 2011, ApJ, 734, 46
Freedman, W. L., Madore, B. F., Scowcroft, V., et al. 2012, ApJ, 758, 24
Gaia Collaboration (Prusti, T., et al.) 2016, A&A, 595, A1
Gaia Collaboration (Clementini, G., et al.) 2017, A&A, 605, A79
Gieren, W., Storm, J., Konorski, P., et al. 2018, A&A, 620, A99
Groenewegen, M. A. T. 2013, A&A, 550, A70
Groenewegen, M. A. T. 2018, A&A, 619, A8
Huang, C. D., Riess, A. G., Yuan, W., et al. 2020, ApJ, 889, 5
Inno, L., Bono, G., Matsunaga, N., et al. 2016, ApJ, 832, 176
Jayasinghe, T., Kochanek, C. S., Stanek, K. Z., et al. 2018, MNRAS, 477, 3145
Kodric, M., Riffeser, A., Hopp, U., et al. 2013, AJ, 145, 106
Leavitt, H. S., & Pickering, E. C. 1912, Harvard College Observatory Circular, 173, 1
Leung, H. W., & Bovy, J. 2019, MNRAS, 489, 2079
Lindegren, L., Hernández, J., Bombrun, A., et al. 2018, A&A, 616, A2
Macri, L. M., Stanek, K. Z., Bersier, D., et al. 2006, ApJ, 652, 1133
Madore, B. F. 1982, ApJ, 253, 575
Marconi, M., Musella, I., & Fiorentino, G. 2005, ApJ, 632, 590
Ngeow, C.-C., Kanbur, S. M., Bellinger, E. P., et al. 2012, Ap&SS, 341, 105
Pejcha, O., & Kochanek, C. S. 2012, ApJ, 748, 107
Pietrzyński, G., Graczyk, D., Gallenne, A., et al. 2019, Nature, 567, 200
Planck Collaboration VI. 2020, A&A, 641, A6
Reid, M. J., Pesce, D. W., & Riess, A. G. 2019, ApJ, 886, L27
Riess, A. G., Macri, L. M., Hoffmann, S. L., et al. 2016, ApJ, 826, 56
Riess, A. G., Casertano, S., Yuan, W., et al. 2018, ApJ, 861, 126
Riess, A. G., Casertano, S., Yuan, W., et al. 2019, ApJ, 876, 85
Ripepi, V., Moretti, M. I., Marconi, M., et al. 2012, MNRAS, 424, 1807
Ripepi, V., Molinaro, R., Musella, I., et al. 2019, A&A, 625, A14
Ripepi, V., Molinaro, R., Marconi, M., et al. 2020, ArXiv e-prints [arXiv:2002.10584]
Romaniello, M., Primas, F., Mottini, M., et al. 2008, A&A, 488, 731
Sandage, A., Tammann, G. A., Saha, A., et al. 2006, ApJ, 653, 843
Shappee, B. J., & Stanek, K. Z. 2011, ApJ, 733, 124
Udalski, A., Soszyński, I., Pietrukowicz, P., et al. 2018, Acta Astron., 68, 315
Yuan, W., Riess, A. G., Macri, L. M., et al. 2019, ApJ, 886, 61
Wong, K. C., Suyu, S. H., Chen, G. C.-F., et al. 2020, MNRAS, 498, 1420